NASA/TM—2011-217123 AHS 2011–000154

Fiber Optic Strain Sensor for Planetary Gear Diagnostics

Jason S. Kiddy
Aither Engineering, Inc., Lanham, Maryland

Paul D. Samuel
Daedalus Flight Systems, LLC, Gaithersburg, Maryland

David G. Lewicki
Glenn Research Center, Cleveland, Ohio

Kelsen E. LaBerge
U.S. Army Research Laboratory, Glenn Research Center, Cleveland, Ohio

Ryan T. Ehinger
Bell Helicopter Textron, Inc., Hurst, Texas

Jason Fetty
U.S. Army Aviation Applied Technology Directorate, Fort Eustis, Virginia

November 2011

NASA STI Program . . . in Profile

Since its founding, NASA has been dedicated to the advancement of aeronautics and space science. The NASA Scientific and Technical Information (STI) program plays a key part in helping NASA maintain this important role.

The NASA STI Program operates under the auspices of the Agency Chief Information Officer. It collects, organizes, provides for archiving, and disseminates NASA's STI. The NASA STI program provides access to the NASA Aeronautics and Space Database and its public interface, the NASA Technical Reports Server, thus providing one of the largest collections of aeronautical and space science STI in the world. Results are published in both non-NASA channels and by NASA in the NASA STI Report Series, which includes the following report types:

- TECHNICAL PUBLICATION. Reports of completed research or a major significant phase of research that present the results of NASA programs and include extensive data or theoretical analysis. Includes compilations of significant scientific and technical data and information deemed to be of continuing reference value. NASA counterpart of peer-reviewed formal professional papers but has less stringent limitations on manuscript length and extent of graphic presentations.

- TECHNICAL MEMORANDUM. Scientific and technical findings that are preliminary or of specialized interest, e.g., quick release reports, working papers, and bibliographies that contain minimal annotation. Does not contain extensive analysis.

- CONTRACTOR REPORT. Scientific and technical findings by NASA-sponsored contractors and grantees.

- CONFERENCE PUBLICATION. Collected papers from scientific and technical conferences, symposia, seminars, or other meetings sponsored or cosponsored by NASA.

- SPECIAL PUBLICATION. Scientific, technical, or historical information from NASA programs, projects, and missions, often concerned with subjects having substantial public interest.

- TECHNICAL TRANSLATION. English-language translations of foreign scientific and technical material pertinent to NASA's mission.

Specialized services also include creating custom thesauri, building customized databases, organizing and publishing research results.

For more information about the NASA STI program, see the following:

- Access the NASA STI program home page at *http://www.sti.nasa.gov*

- E-mail your question via the Internet to *help@sti.nasa.gov*

- Fax your question to the NASA STI Help Desk at 443–757–5803

- Telephone the NASA STI Help Desk at 443–757–5802

- Write to:
  NASA Center for AeroSpace Information (CASI)
  7115 Standard Drive
  Hanover, MD 21076–1320

NASA/TM—2011-217123 AHS 2011–000154

Fiber Optic Strain Sensor for Planetary Gear Diagnostics

Jason S. Kiddy
Aither Engineering, Inc., Lanham, Maryland

Paul D. Samuel
Daedalus Flight Systems, LLC, Gaithersburg, Maryland

David G. Lewicki
Glenn Research Center, Cleveland, Ohio

Kelsen E. LaBerge
U.S. Army Research Laboratory, Glenn Research Center, Cleveland, Ohio

Ryan T. Ehinger
Bell Helicopter Textron, Inc., Hurst, Texas

Jason Fetty
U.S. Army Aviation Applied Technology Directorate, Fort Eustis, Virginia

Prepared for the
67th Annual Forum and Technology Display (Forum 67)
sponsored by the American Helicopter Society (AHS)
Virginia Beach, Virginia, May 3–5, 2011

National Aeronautics and
Space Administration

Glenn Research Center
Cleveland, Ohio 44135

November 2011

Acknowledgments

This research was partially funded by the Government under Agreement No. W911W6-07-2-0003.

Level of Review: This material has been technically reviewed by technical management.

Available from

NASA Center for Aerospace Information
7115 Standard Drive
Hanover, MD 21076–1320

National Technical Information Service
5301 Shawnee Road
Alexandria, VA 22312

Available electronically at http://www.sti.nasa.gov

Fiber Optic Strain Sensor for Planetary Gear Diagnostics

Jason S. Kiddy
Aither Engineering, Inc.
Lanham, Maryland 20706

Paul D. Samuel
Daedalus Flight Systems, LLC
Gaithersburg, Maryland 20877

David G. Lewicki
National Aeronautics and Space Administration
Glenn Research Center
Cleveland, Ohio 44135

Kelsen E. LaBerge
U.S. Army Research Laboratory
Glenn Research Center
Cleveland, Ohio 44135

Ryan T. Ehinger
Bell Helicopter Textron Inc.
Hurst, Texas 76053

Jason Fetty
U.S. Army Aviation Applied Technology Directorate
Fort Eustis, Virginia 23604

Abstract

This paper presents a new sensing approach for helicopter damage detection in the planetary stage of a helicopter transmission based on a fiber optic strain sensor array. Complete helicopter transmission damage detection has proven itself a difficult task due to the complex geometry of the planetary reduction stage. The crowded and complex nature of the gearbox interior does not allow for attachment of sensors within the rotating frame. Hence, traditional vibration-based diagnostics are instead based on measurements from externally mounted sensors, typically accelerometers, fixed to the gearbox exterior. However, this type of sensor is susceptible to a number of external disturbances that can corrupt the data, leading to false positives or missed detection of potentially catastrophic faults. Fiber optic strain sensors represent an appealing alternative to the accelerometer. Their small size and multiplexibility allows for potentially greater sensing resolution and accuracy, as well as redundancy, when employed as an array of sensors. The work presented in this paper is focused on the detection of gear damage in the planetary stage of a helicopter transmission using a fiber optic strain sensor band. The sensor band includes an array of 13 strain sensors, and is mounted on the ring gear of a Bell Helicopter OH-58C transmission. Data collected from the sensor array is compared to accelerometer data, and the damage detection results are presented.

Introduction

In recent years, much research has been devoted to the development of Health and Usage Monitoring Systems (HUMs) for rotorcraft. The promise of HUMS is the ability to provide accurate information regarding the condition of various flight critical components, enabling scheduled maintenance intervals to be increased and minimize the number of parts decommissioned before the end of their useful life, and thus reducing operating costs associated with civilian and military helicopters. In addition, an increase in helicopter safety and reliability could be realized.

The transmission is one of the significant flight critical components within the helicopter, and a large portion of helicopter transmission HUMS research has been focused on the use of vibration-based damage detection techniques. These techniques are applied to vibration signals collected from vibration transducers, typically accelerometers. Helicopters use a planetary gearbox as the final stage of the transmission. The detection of damage within helicopter transmissions has proven to be a particularly difficult task. The crowded and complex nature of the planetary gearbox interior does not allow for robust attachment of sensors within the rotating frame. Hence, traditional vibration-based diagnostics are instead based on measurements from externally-mounted accelerometers fixed to the gearbox exterior. Advanced processing of this global vibration data provided by the

accelerometers can enhance the appearance of signal anomalies that indicate the presence of damage within the gearbox.

Much effort has been focused on the use of accelerometer vibration data for helicopter transmission damage detection (Refs. 1 to 3). However, this type of sensor is susceptible to a number of external disturbances that can corrupt the data, leading to false positives or missed detection of potentially catastrophic faults.

Fiber optic strain sensors represent an appealing alternative to the accelerometer due to their resistance to electromagnetic interference and other signal corrupting influences. Their small size and multiplexibility allows for potentially greater sensing resolution and accuracy, as well as redundancy, when employed as an array of sensors.

Researchers have established the capability of fiber optic sensors for structural health and usage monitoring systems (Ref. 4), but their use with dynamic systems has been limited. The use of fiber optic strain sensors to detect damage in the internal components of a helicopter transmission is an emerging area of research and thus few results have been published to date.

The feasibility of such a system to detect planetary gearbox damage has been only recently demonstrated (Ref. 5), and signal processing techniques that enhance the appearance of such damage are in their infancy (Refs. 6 and 7).

The work presented in this paper is focused on the detection of gear damage in the planetary stage of a helicopter transmission using a fiber optic strain sensor band. The sensor band includes an array of 13 strain sensors, and is mounted on the ring gear of a Bell Helicopter OH-58C transmission. Data collected from the sensor array is compared to accelerometer data, and the damage detection results are presented.

NASA Glenn OH-58 Test Stand

The tests were performed in the NASA Glenn Research Center 500-hp helicopter transmission test facility using an OH-58C helicopter main-rotor transmission, as shown in Figure 1. The test stand operates on the closed-loop or torque-regenerative principle. Mechanical power recirculates through a closed loop of gears and shafting, part of which is the test transmission. A 200-hp variable-speed direct-current (DC) motor powers the test stand and controls the speed. A 15-hp DC motor provides the torque in the closed loop. A mast shaft loading system in the test stand simulates rotor loads imposed on the OH-58C transmission output mast shaft. The OH-58C transmission output mast shaft connects to a loading yoke. Two vertical load cylinders connected to the yoke produce lift loads. A single horizontal load cylinder connected to the yoke produces a bending load (Ref. 8).

Fiber Optic Strain Sensors

Fiber Bragg Gratings (FBGs) have become an integral part of the telecommunications hardware, used in applications such as add/drop filters, fiber lasers, and data multiplexing (Ref. 9).

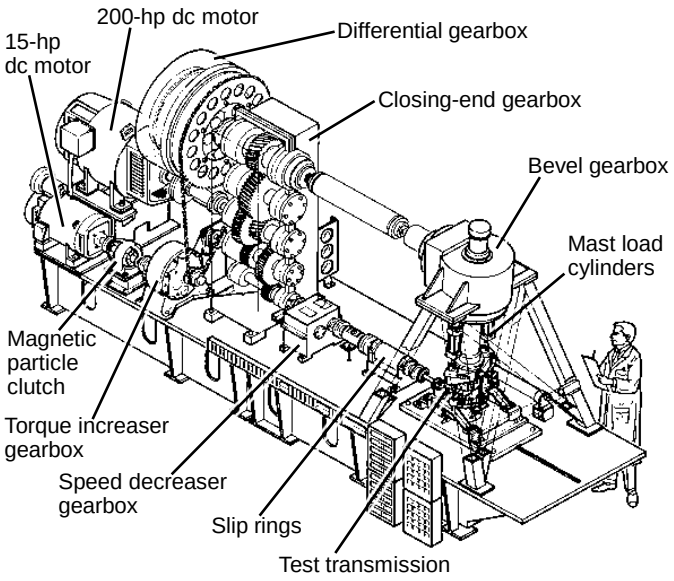

Figure 1.—NASA Glenn 500 Horsepower Helicopter Transmission Test Facility.

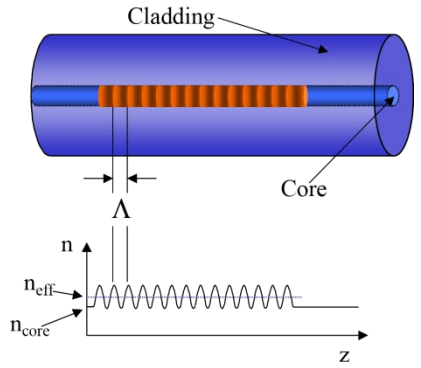

Figure 2.—Schematic of a fiber Bragg grating.

As shown in Figure 2, the FBG sensor is fabricated by altering the refractive index, *n*, of the core of an optical fiber in a periodic fashion, creating a Bragg grating that reflects a specific wavelength of light, referred to as the Bragg wavelength.

The period of the change is referred to as the grating pitch. Both the effective refractive index of the core and the grating pitch vary with changes in strain and temperature, so that the Bragg wavelength shifts to higher or lower wavelengths in response to applied thermal-mechanical fields. For most applications including the transmission monitoring system, the shift in the Bragg wavelength is considered a linear function of the thermal-mechanical load. In addition, for the present application, the thermal response of the system is much slower than the expected mechanical response and thus can be easily filtered out. Hence, a strain-based vibration signal can be measured by recording the changes in the wavelength of the light reflected from a given FBG as shown in the following equation. In this equation, λ_B is the Bragg wavelength, P_e is a constant scaling term, and ε_z is the longitudinal strain in the direction of the fiber.

$$\frac{\Delta\lambda_B}{\lambda_B} = P_e \varepsilon_z$$

The optical response of an FBG sensor is wavelength encoded allowing many FBG sensors to be serially multiplexed via wavelength division multiplexing techniques. Each FBG reflects a different wavelength, and sufficient space is provided so that strain does not cause the wavelength of the light reflected from two separate sensors to overlap when strained. The space required as well as the wavelength range of the interrogator box limit the number of sensors. Many commercially available interrogation systems have come to market making these types of sensors and systems readily available to the end user.

FBG Strain Sensor Array Band

For this research, an array of 13 FBG strain sensors was mounted on a tension band clamp as shown in Figure 3. Previous testing has shown that good strain transfer can be obtained with the clamp mounted to the outside of a ring gear (Refs. 6 and 7). The advantage of the band clamp is that it relatively easy to install and remove as necessary.

The OH-58C ring gear is secured to the transmission housing with the use of splined teeth along the outside edge of the ring gear that mate with corresponding splines on the transmission housing. Therefore, modifications to both the ring gear and transmission housing were needed.

The modifications to the ring gear itself were two-fold. First, a section of the spline teeth along the entire circumference of the gear was removed to allow for the sensor band to be strapped to the outside. And second, two smaller portions had the spline teeth completely removed to allow for the optical fiber to egress off of the ring gear and onto the top of the transmission case where it exited from the transmission. The ring gear was modified as shown in Figure 4.

There were three main modifications to the transmission housing that were required. The first was to machine a section near the mounting bracket to allow for the band clamp tensioning mechanism. The second was to machine away some of the spline teeth for the fiber to egress off of the band and then to the top of the housing, and the third was to add a groove in the oil port to allow the fiber to exit the transmission. Additional modifications were necessary to secure the optical cable to the top of the housing; those were made in-house following the more intensive machining processes. The modified housing is shown in Figure 5.

Fiber Optic Strain Sensor and Corresponding Accelerometer Locations

After assessing several possible accelerometer and fiber optic sensor locations, the final placement was selected. The final fiber optic sensor and accelerometer locations are listed in Table I, and shown in Figure 6. Note that in Sensor

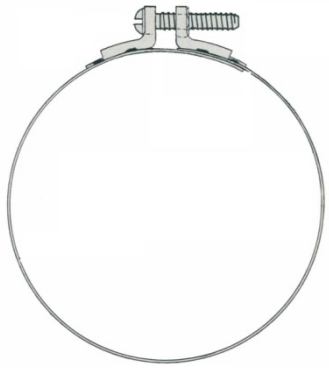

Figure 3.—Band clamp schematic.

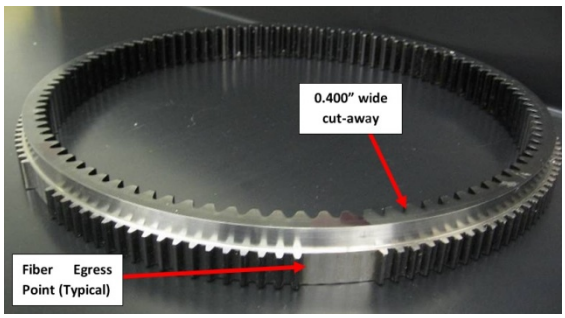

Figure 4.—Modified OH-58C ring gear.

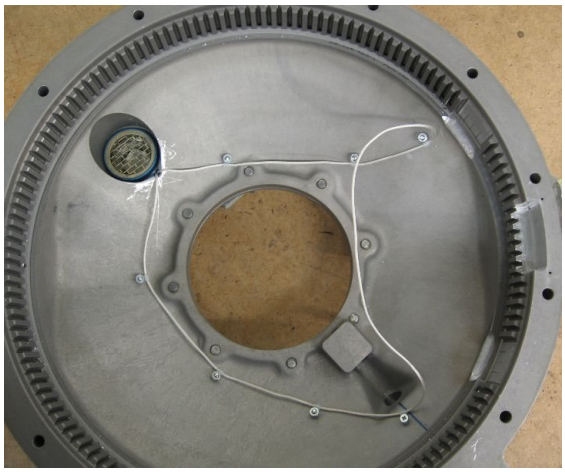

Figure 5.—Transmission housing modifications.

Region 1, the two secondary fiber optic sensors were designed to be half the length of standard FBG sensors, about 5 mm versus 1cm for standard FBGs. Although the optical properties suffer slightly, the shorter sensors were used to determine if a strain gradient across the sensor affected their performance. Although not discussed in detail in this paper, the difference was minimal and standard FBGs performed adequately. For the set of fiber optic sensor locations, stud-mounted accelerometers were aligned with the primary fiber sensors in regions 2 and 3 at teeth 9 and 71, respectively. In addition, a bracket-mounted accelerometer was mounted on the bolt in region 1, which is near tooth 40.

TABLE I.—FINAL FIBER OPTIC SENSOR LOCATIONS (0.5 L INDICATES 5 mm SENSOR)

Sensor	Ring tooth referenced location: Sensor Region 1 (Planet Tooth 1)	Ring tooth referenced location: Sensor Region 2 (Planet Tooth 34)	Ring tooth referenced location: Sensor Region 3 (Planet Tooth 32)
Primary fiber optic sensor	40	9	71
Secondary fiber optic sensors	39 (0.5 L), 41 (0.5 L)	7, 8, 10, 11	70, 70.5, 71.5, 72
Accelerometer	40 (bracket-mounted on nearest bolt)	9 (stud-mounted)	71 (stud-mounted)

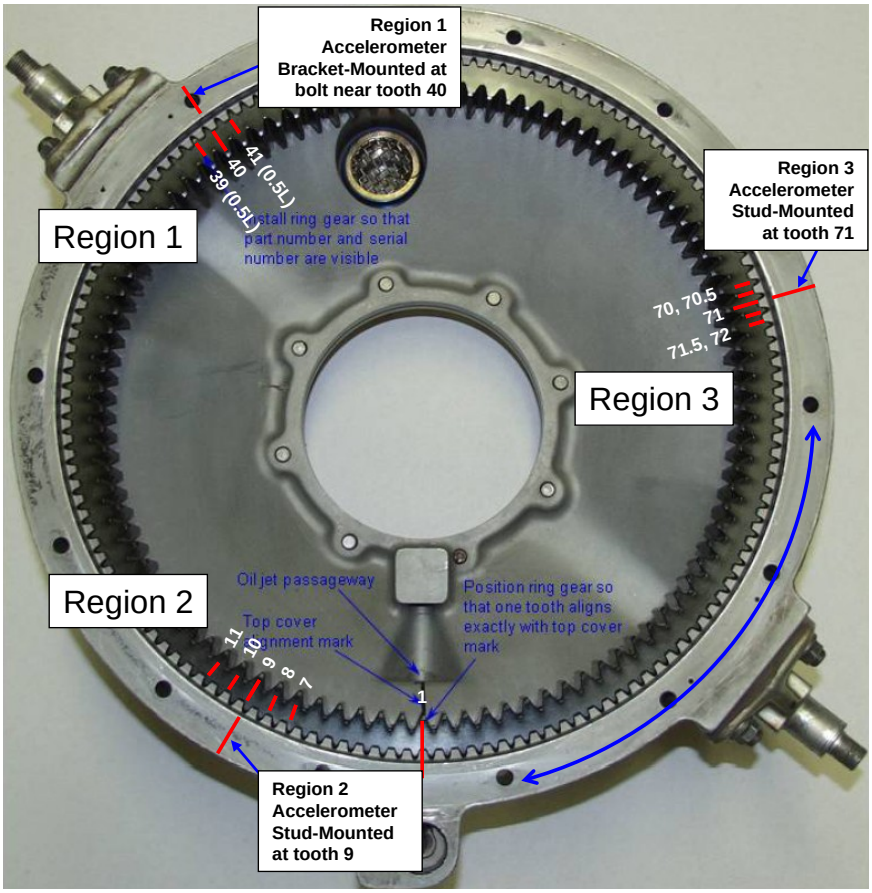

Figure 6.—Final FO sensor and accelerometer locations.

The optical fiber selected was polyimide coated. A polyimide coating, as opposed to the more standard acrylate coating, gives higher temperature performance at the expense of being a bit more difficult to handle due to its smaller size and higher susceptibility to optical bend losses. The optical fiber was bonded to the clamp using conventional strain gauge epoxy, Vishay Measurements Group AE-10. The fiber was bonded along the entire length of the band clamp with the exception of a region within a couple of inches from each of the tensioning brackets. In those regions, small-diameter fiberglass jacketing made by Varflex, Inc. was slid over the fiber and also bonded in place. The Varflex helps protect the egress location. Additional thicker cabling was then added to further protect the fiber as it runs along the top cover and out of the transmission. Upon installation, portions of the cable at the band clamp tensioning bracking and exiting the oil fill port were coated with silicon rubber to secure the optical fiber cabling. The band sensor cable is approximately 1 m long at which point it terminates in a standard telecommunications FC/PC connector. From this point a standard fiber optic patchcord connects the sensor to the instrumentation in the control room.

Experimental Procedure

The major goal of the project was to study data collected at the NASA Glenn Research Center OH-58 transmission test rig facility from the fiber optic ring gear sensor array. First, the healthy data was evaluated to determine the fundamental characteristics of the OH-58C transmission strain signal waveform. Second, damage data was evaluated to determine how various types of damage are manifested in the OH-58C

strain signal. An initial evaluation was used to determine the effectiveness of existing damage detection algorithms and to select a damage detection approach. After determination of the damage detection approach, the damage data was evaluated to ascertain how each type of damage is manifested in the signal, and how well each type of damage could be detected using the selected approach. Third, the effect of torque variation and mast loading on the strain signal waveform as well as on the damage-detection performance was investigated.

The damaged test cases that were considered are as follows:

- 1-1: Baseline test
- 1-2A: Planet pinion root crack, 25 percent depth, sun-side crack opening
- 1-2B: Planet Pinion root crack, 25 percent depth, ring-side crack opening
- 1-3A: Planet pinion root crack, 50 percent depth, sun-side crack opening
- 1-3B: Planet pinion root crack, 50 percent depth, ring-side crack opening
- 1-4A: Planetary pinion tooth spalled at the pitch line, sun-side
- 1-4B: Planetary pinion tooth spalled at the pitch line, ring-side
- 1-5: Sun gear root crack, 25 percent depth
- 1-6: Sun gear tooth spalled at the pitch line
- 1-7: Ring gear root crack, 25 percent depth
- 1-8: Ring gear root crack, 50 percent depth
- 1-9: Planet bearing outer race pitting
- 1-10: Planet bearing inner race pitting

The fiber optic instrumentation used during this program, Micron Optics sm130 interrogator, had a maximum sampling rate of 1,000 Hz. Standard operating speed of the input shaft to the transmission is 6,180 rpm. However, at that speed the fiber optic instrumentation would be unable to resolve individual tooth meshes. Therefore, the transmission was operated at 2,060 rpm for the fiber optic testing. Data collection was performed for each test condition; damage case, torque level, mast loading on/off, for a total of 30 hunting tooth cycles. The hunting tooth cycle is defined as the period in which the position of all planetary gear teeth repeats, and is defined in the OH-58 transmission as 105 output rotations.

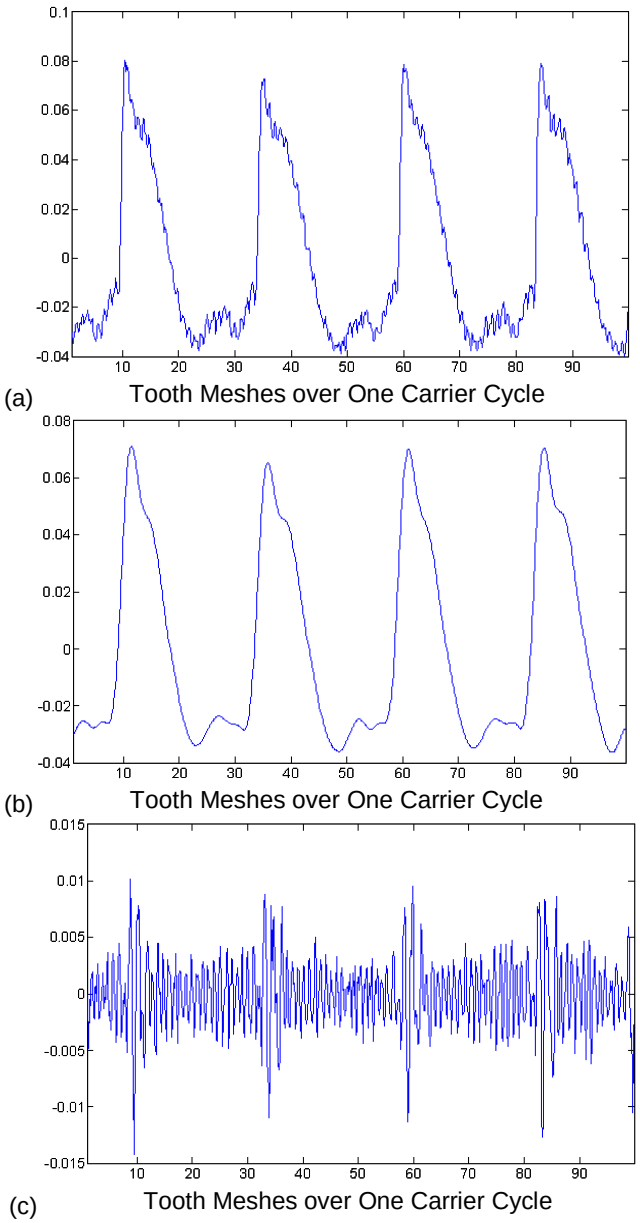

Figure 7.—Healthy vibration data collected from the OH-58C transmission using a fiber optic strain sensor. (a) Raw data, (b) low frequency component, (c) high frequency component.

Data Analysis

Initially, the strain data was inspected and it was determined that the signal was composed of two primary components, one low frequency, large amplitude component associated with the deformation of the ring during planet passes and a second high frequency small amplitude component associated with local tooth deformation. A technique for separating the two components was developed based on standard high/low pass filtering. A representative raw strain signal and the resulting separated components are shown in Figure 7.

Signal-to-Noise Ratio

A comparison of signals from a strain sensor and a collocated accelerometer revealed that the raw strain signal had a significantly higher signal-to-noise ratio than the raw accelerometer signal as shown in Figure 8.

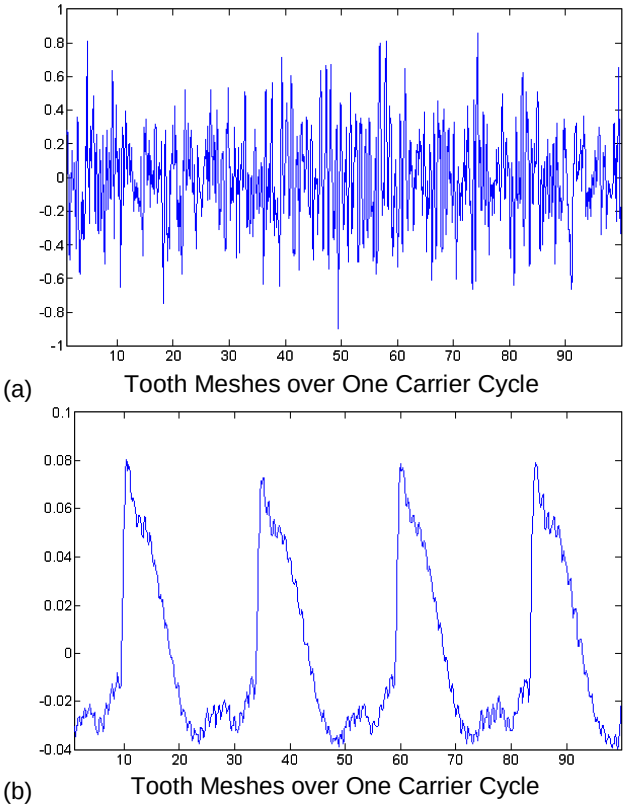

Figure 8.—Healthy vibration data collected from the NGRC OH-58 transmission using (a) an accelerometer and (b) a collocated fiber optic strain sensor.

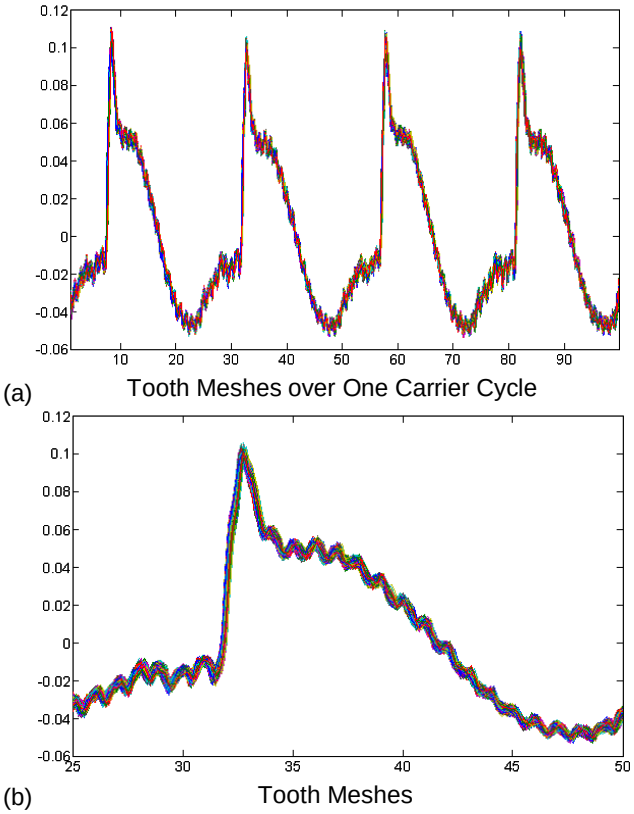

Figure 9.—(a) Overlay of 1200 carrier cycles of strain data from fiber optic strain sensor no. 1. (b) Close-up of one planet pass lobe.

Uncertainty Analysis

Further evaluation of the OH-58C strain data shows that the variation in the signal waveform appears to be exceptionally low from cycle-to-cycle. Figure 9 shows an overlay of 1200 consecutive carrier cycles of strain data from a representative fiber optic strain sensor (strain sensor no. 1). The consistency of the waveform is evident as both the underlying ring strain signal and the individual tooth strain signals are clearly visible even when 1200 individual signals are overlaid.

Based on this consistency, our research shows that it is not necessary to average the data as is required for accelerometer data. Instead, it is possible that the condition indicators (CIs) may be applied directly to the unaveraged signal. This would significantly reduce the amount of data required to compute the various CIs and the amount of data gathering time needed to collect adequate data.

Considering that helicopter operations rarely stay in a particular flight condition for long, the sensor consistency coupled with multiple FBG sensors on a single array can greatly improve data quality by quickly gathering all of the required data in a much shorter period of time compared to accelerometers. For this study, both un-averaged and averaged data were analyzed.

Vibration Separation

Vibration separation is a synchronous averaging technique that extracts individual vibration signals for the sun gear and each of the planet gears from the raw planetary gearbox vibration signal (Refs. 10 to 12). Since vibration separation is a form of synchronous averaging, it serves to enhance the features associated with the gear of interest while suppressing features associated with other components as well as noise. However, vibration separation has the added benefit that it indexes the teeth of the gear and assembles a signal associated with that gear that can more easily be used for damage detection.

As mentioned earlier, planetary gearbox vibration transducers are typically mounted on the gearbox housing, and are fixed relative to the moving planet gears and sun gear. When a planet passes close to a transducer, the amplitude of vibration measured by that transducer increases. The result is a region of increased amplitude, or a lobe, in the vibration signal associated with the passing of each planet. These lobes are clearly visible in the high frequency component of the fiber optic strain signal shown in Figure 7(c). Thus, data collected during one rotation of the planetary carrier will have a lobe for each planet; these lobes are often referred to as planet-pass lobes.

The vibration separation algorithm relies on two assumptions.

1. The vibrations in each lobe region are predominately generated by the local planet gear meshing with the sun and ring gear.
2. A hunting tooth ratio exists for the planet/ring gear pair and the sun/ring gear pair.

Given these assumptions, the vibration separation algorithm can be summarized in the following three steps.

1. A window is applied to each lobe to capture the segment of the signal dominated by the local planet gear.
2. The known geometry of the gearbox is used to index and arrange the windows sequentially according to either the progression of planet or sun teeth.
3. The windows are then assembled into a single vibration signal for each planet and for the sun.

Another key requirement for application of the vibration separation algorithm is that the raw vibration signal for each carrier cycle must have the same number of samples. Even small variations in the gearbox rpm will lead to a different number of samples in each carrier cycle signal. Thus, the data is interpolated (up-sampled) such that each tooth mesh is represented by 2^n points. The value of n is chosen such that 2^n is the smallest number of points greater than that of the original data. This choice aids in the efficiency of the processing. The effect of various interpolation techniques on transmission vibration data has been studied and shown to be minimal (Ref. 13). While down-sampling is generally preferred, up-sampling is required in this case due to the low sampling frequency of the data. Thus, care is required in subsequent analysis of the data to ensure that high frequency features above the Nyquist frequency of the raw data are identified as artifacts of the processing rather than actual signal features.

A detailed description of the vibration separation algorithm is presented in References 10 to 12. However, it should be noted that in addition to suppressing non-salient features, the vibration separation algorithm also directly eliminates portions of the signal (through windowing) that do not contain salient information.

The primary variables in the implementation of the algorithm are the width and shape of the window applied to the planet pass lobes. In past work, it was found that for accelerometer vibration signals, a 4/5 Tukey window (total width of 5 tooth meshes, flat center region of 1 tooth mesh and Gaussian tails of 2 tooth meshes on either side of flat center) produced the best representation of the planetary vibration signal (Ref. 11). During assembly, the tails of the 4/5 Tukey window overlap the two adjacent windows on either side. This overlap serves to minimize any discontinuities between data segments, as well as reinforcing the planetary vibration components through averaging. The indexing and arrangement of the windows ensures that vibration data segments generated by a given planet tooth are averaged only with other vibration data segments generated by the same tooth.

Given the differences between the accelerometer data and the fiber optic strain data, it was not clear that the same window was appropriate for both types of data. It was hypothesized that the clean nature of the data would either increase the useful data in the tails of the planet pass lobe, or would reduce the size of discontinuities, enabling a smaller window with shorter tails to be used. Hence, three windows were chosen for evaluation.

1. Original Window: 4/5 Tukey window with a width of 5 tooth meshes.
2. Wide Window: 3/5 Tukey window with a total width of 10 tooth meshes.
3. Narrow Window: 1/3 Tukey window with a width of 1.5 tooth meshes.

The undamaged high-frequency component of the strain data was processed using the vibration separation algorithm with each of the three windows to generate planet vibration signals, and the frequency spectrum of the resulting planetary signals was evaluated and it was determined that the 10 tooth mesh window provided the most accurate reconstructed planetary signal. The 10 mesh wide window resulted in the lowest signal-to-noise ratio, and successfully captured the mesh frequency and first harmonic. The 5 mesh wide window had a higher signal-to-noise ratio and failed to capture the first harmonic. The 1.5 mesh wide window had a similar signal-to-noise ratio as the 5 mesh wide window, and indicated a 3rd and even 4th harmonic in addition to harmonics 1 and 2. As mentioned above, window overlap minimizes the discontinuities between adjacent signal segments. If the discontinuities are not sufficiently attenuated, then high frequency harmonics result. Recall that the earlier up-sampling would make it possible to see high frequency features not present in the original raw data. Given that the Nyquist frequency of the original raw data is between the second and third harmonics, any indication of a harmonic higher than the 2nd is an artifact of the assembly process. Since the 1.5 mesh wide window shows both a 2nd and 3rd harmonic, it is clear that it does not sufficiently attenuate the discontinuities. Thus, the 10 tooth mesh wide window was chosen for this research.

Once a separated vibration signal has been assembled, it is typically averaged with subsequent assembled vibration signals. However, as mentioned previously, further averaging of the strain data may not be necessary, and thus both unaveraged and averaged assembled signals were analyzed.

Damage Detection Results

A number of basic damage detection metrics were then computed using the resulting separated signals. For this case, 30 subsequent separated signals were averaged. The condition indicators included in this project were the Kurtosis, FM0, FM4, M6A, M8A, the RMS Energy, the Crest Factor (CF), the Energy Operator (EO), and the Energy Ratio (ER). A summary of the metric description is provided in Reference 3.

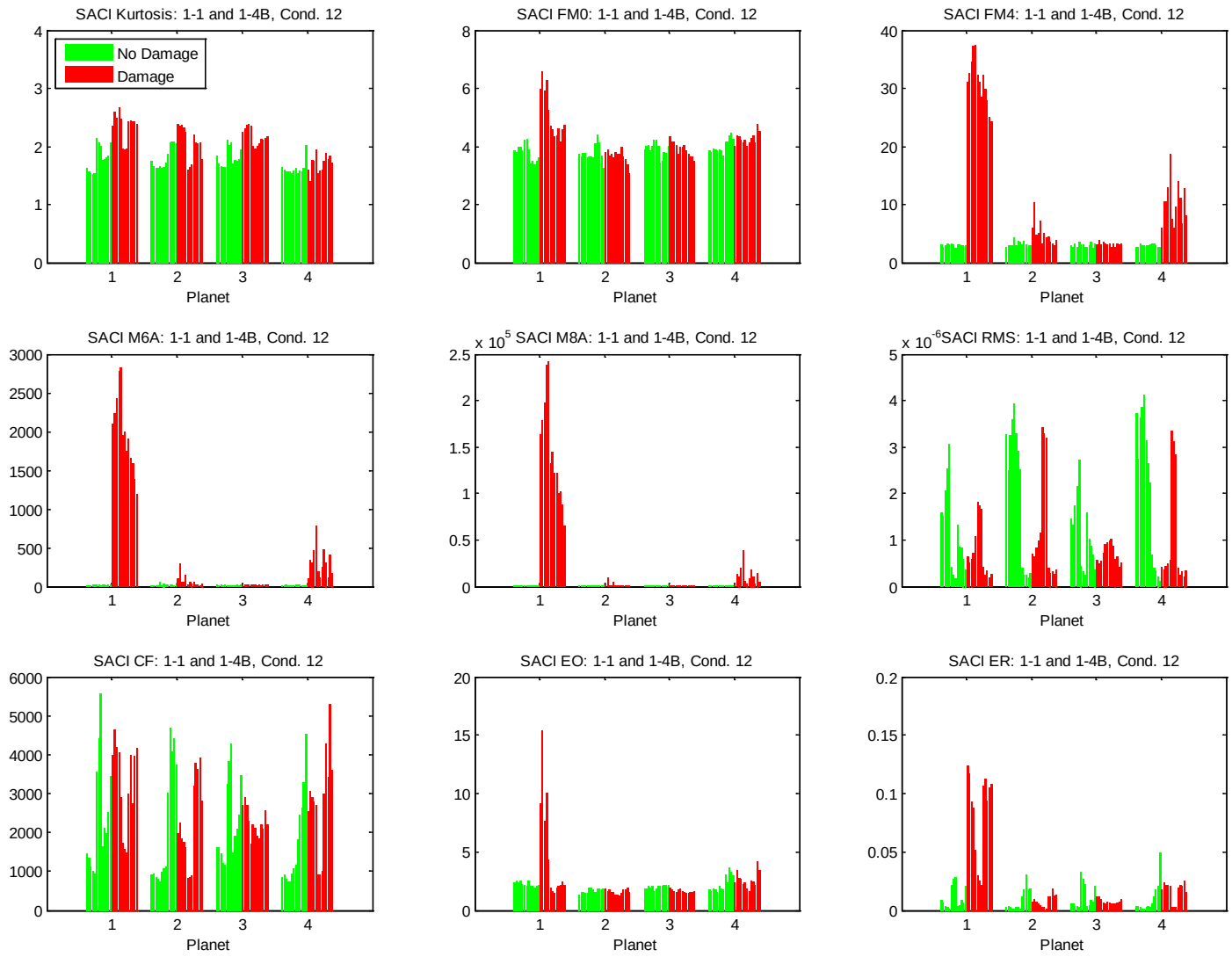

Figure 10.—Comparison of signal averaged condition indicator (SACI) values for the undamaged (green bars/left side) and the planet pinion tooth pitch line spall, ring-side (red bars/right side). Sensors 1-13 are shown for each planet.

As an example, the detection result for the planet tooth spall is shown in Figure 10. In this figure the increased amplitude of the red bars (right side of each planet response) over the amplitude of the baseline green bars (left side for each planet) for multiple metrics clearly indicates the damage on Planet 1. Specifically, FM4, M6A, M8A, and ER provide a strong indication of damage on Planet 1. In addition, FM0 and EO provide a weaker, though still clear, indication that the damage is on Planet 1.

From Figure 10, a large variation can be seen between different strain sensor locations. This may be caused by several factors, including the geometry of the transmission housing, location of the strain sensors relative to the ring gear teeth and the splines, band tension variability and fiber bonding variability. Overall, results from the damage detection analysis, by visually interpreting graphs similar to those shown in Figure 10 are shown in Table II.

For damage cases 1-5 and 1-6, pertaining to sun gear damage, the lack of detection capability is believed to be caused primarily because there is no hunting tooth ratio for relating sun gear teeth to the ring gear sensor position. The distance between the damage and the strain sensor location may also contribute to the lack of sensitivity. For the ring gear damage cases, 1-7 and 1-8, the no detection result was surprising to the authors.

It should be noted that this was an effort to assess the effectiveness for fiber optic strain monitoring and further optimization could be performed. Although some damage cases are listed as Marginal Confidence or No Detection, future efforts to improve the analysis and generate potentially new condition indicators specific to fiber optic strain-based sensors may improve the detection capability. Furthermore, advances in the fiber optic data collection instrumentation to allow for higher sampling rates will improve the likelihood of detecting some faults, specifically the bearing damage cases which are known to generate high frequency signals above those measured in this project.

TABLE II.—CONFIDENCE IN THE DAMAGE DETECTION RESULT FOR EACH DAMAGE CASE

Case	Suggested confidence
1-2A: Planet pinion root crack, 25% depth, sun-side crack opening	Moderate confidence
1-2B: Planet pinion root crack, 25% depth, ring-side crack opening	Marginal confidence
1-3A: Planet pinion root crack, 50% depth, sun-side crack opening	High confidence
1-3B: Planet pinion root crack, 50% depth, ring-side crack opening	High confidence
1-4A: Planet pinion pitch line tooth spall, sun-side contact	Moderate confidence
1-4B: Planet pinion pitch line tooth spall, ring-side contact	High confidence
1-5: Sun gear root crack, 25% depth	No detection
1-6: Sun gear pitch line tooth spall	No detection
1-7: Ring gear root crack, 25% depth	No detection
1-8: Ring gear root crack, 50% depth	No detection
1-9: Planet bearing outer race pitting	No detection
1-10: Planet bearing inner race pitting	No detection

Effect of Averaging

The results presented above consider the case where 30 separated signals are averaged prior to applying the condition indicators. As mentioned previously, the high signal-to-noise and repeatability of the strain-based measurements provides an opportunity to consider applying the damage metrics to a single separated signal. In Figure 11, the data is processed in this manner, with the condition indicators being averaged over the number of planet passes, as opposed to the vibration data being averaged prior to application of the indicators. The condition indicators are averaged to enable a concise display of results, and the one-sigma error is indicated to show the distribution. For actual application, the condition indicators would not be averaged, but instead would be evaluated as they are computed.

It appears from Figure 11 that for this damage case, some of the averaged condition indicators may provide an indication of the presence of damage as well. Specifically, FM4, M6A and M8A appear to indicate damage. Hence, it is possible that condition indicators computed using unaveraged data could be used as an early indication of tooth spalling for teeth that come in contact with the ring gear. If the unaveraged condition indicator indicates damage, then more data could be collected and averaged to improve confidence in the detection result.

Torque Sensitivity

For every test case investigated in this project, data for four torque levels was collected. For all of the previous analysis, the highest torque level was used. This section focuses on the effect of changes in the torque level on the fiber optic strain vibration signals.

Figure 12(a) shows unaveraged vibration signals for the four torque levels for a single carrier cycle. Figure 12(b) shows the low frequency component of the signals, and Figure 12(c) shows the high frequency component of the signals. From these figures, it is evident that a change in torque has a clear effect on the amplitude of the vibration signal, as expected. However, comparing the low frequency and high frequency components, it appears that the effect on the amplitude of the low frequency ring deformation component is much greater than the effect on the amplitude of the high frequency tooth deformation component.

This result suggests that the amplitude, either peak-to-peak or maximum, of the low frequency component of the strain signal could be correlated with the torque load on the transmission. This could be useful for direct usage monitoring.

As noted above, the effect of torque variation on the amplitude of the high frequency component of the strain signal is much smaller than on the low frequency component. However, this does not necessarily imply that damage detection performance will be unaffected. To evaluate the effect of torque variation on damage detection, the damage case which consists of a spall at the pitch line on the face of a single planet pinion tooth is selected for comparison with the baseline case 1-1. For this evaluation, the low torque data set is shown.

Figure 13 shows each of the condition indicator values for each planet compared with the undamaged baseline values for each planet. It is evident that this damage case can still be detected. However, the indication is not nearly as strong as in the high torque case shown in Figure 10.

Overall, these results indicate that the performance of the damage detection methodology may be affected by variations in torque and that a significant reduction in torque is detrimental to the damage detection performance even though the effect on the amplitude of the high frequency signal is minimal. However, it is possible that the torque sensitivity could be used to monitor the transmission torque, or more directly component strain, in real time and serve as input to a remaining useful life algorithm for usage monitoring. Thus it is recommended that the use of the low frequency signal for remaining useful life estimation be studied in a future research program.

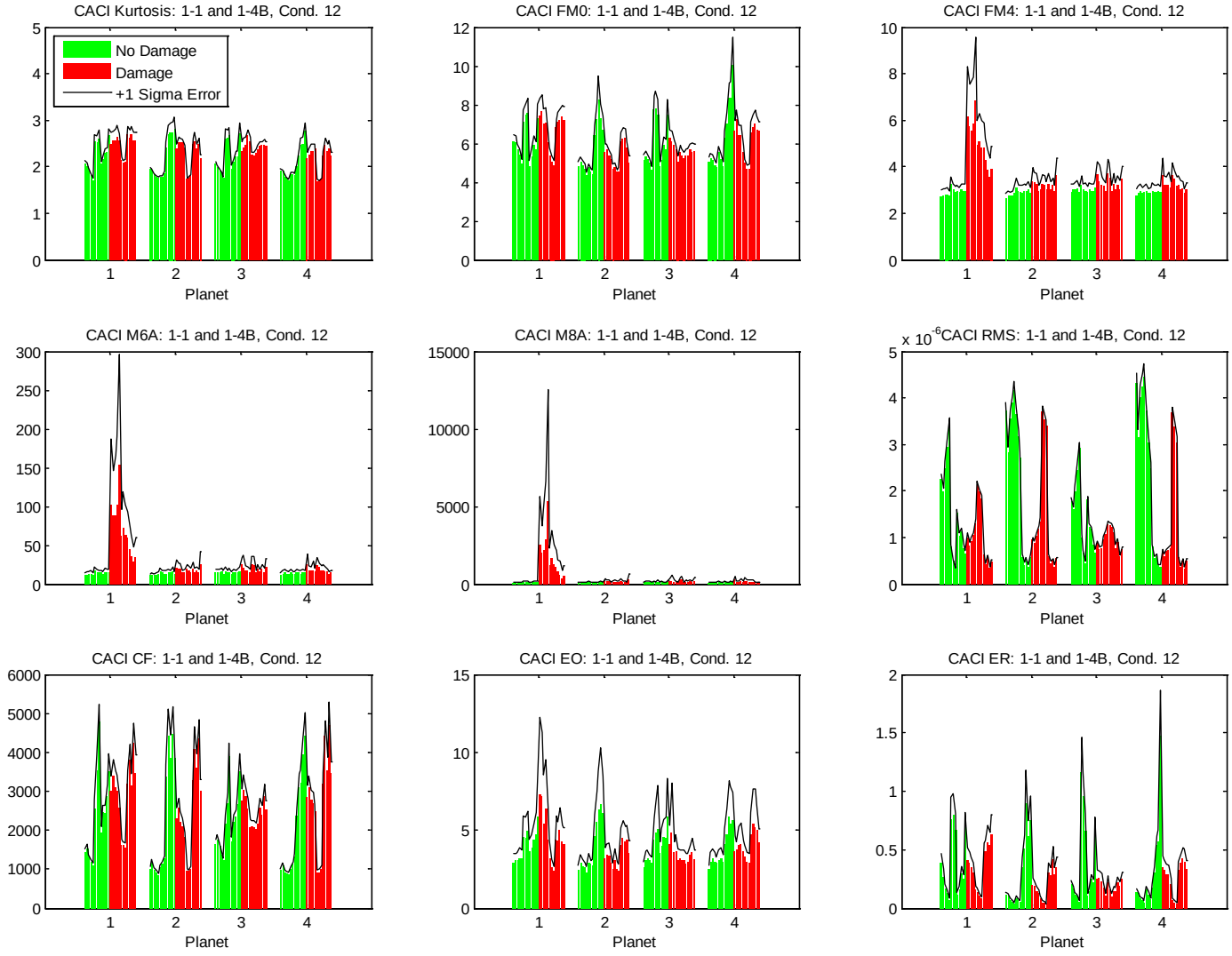

Figure 11.—Comparison of CI averaged condition indicator (CACI) values for the undamaged case (green bars/left side) and the planet pinion tooth pitch line spall, ring-side case (red bars/right side). Positive 1-σ error is Indicated by the black line. Sensors 1 - 13 are shown for each planet

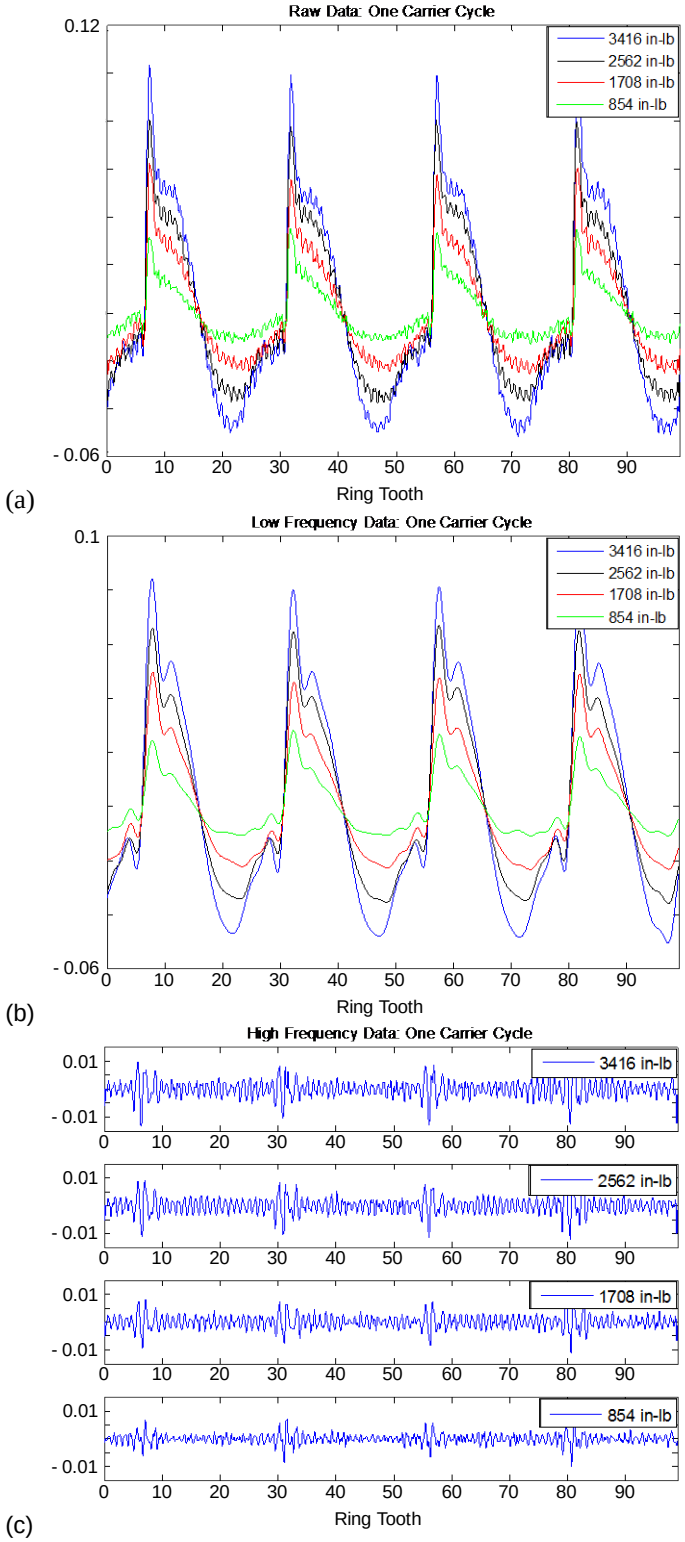

Figure 12.—Comparison of one carrier cycle for four different torque levels, (a) Raw signal, (b) low frequency vibration signal component, (c) high frequency vibration signal component.

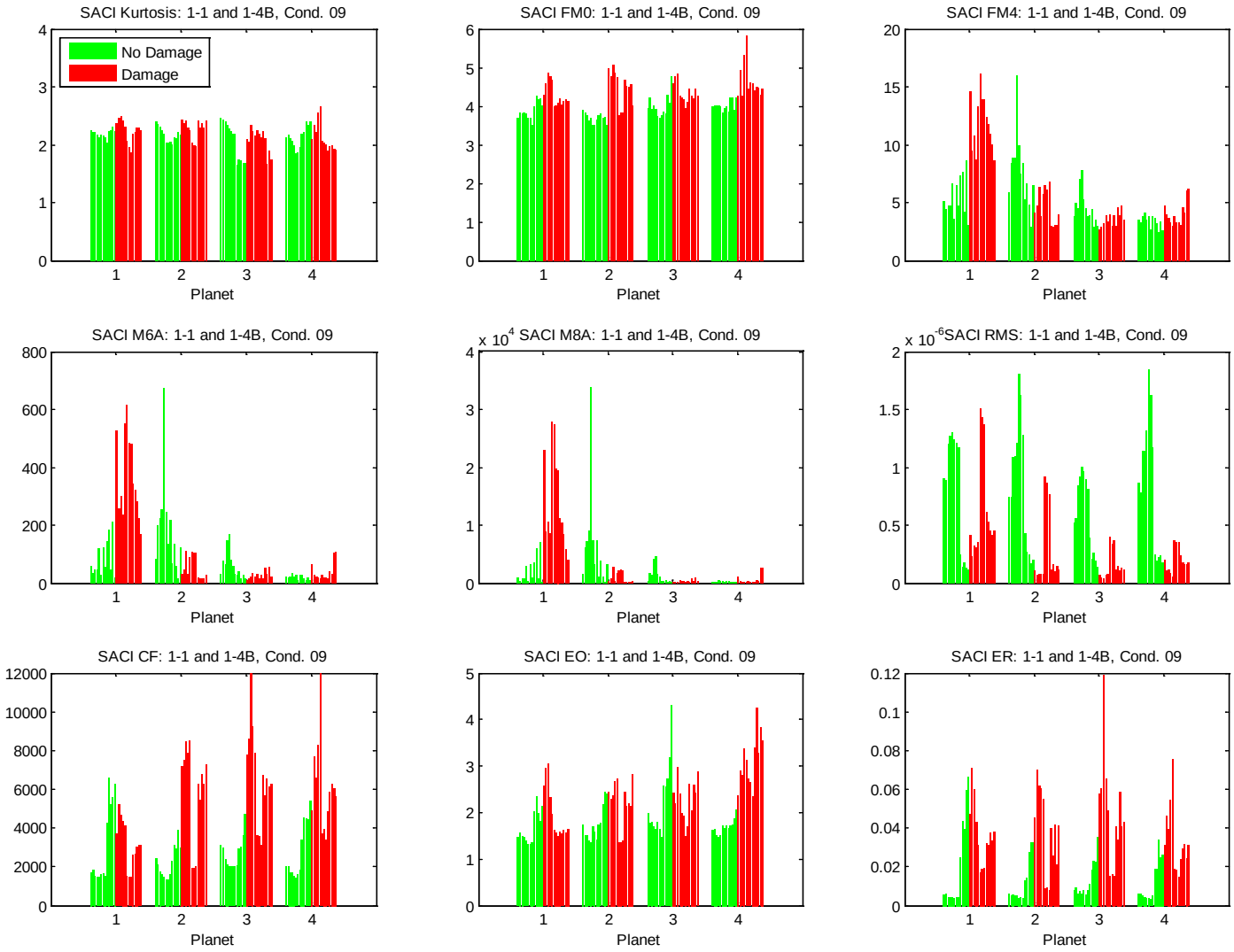

Figure 13.—Comparison of signal averaged condition indicator (SACI) values for low torque (854 in-lb) condition for the undamaged case (green bars/left side) and the planet pinion tooth pitch line spall, ring-side case (red bars/right side). Sensors 1 - 13 are shown for each planet.

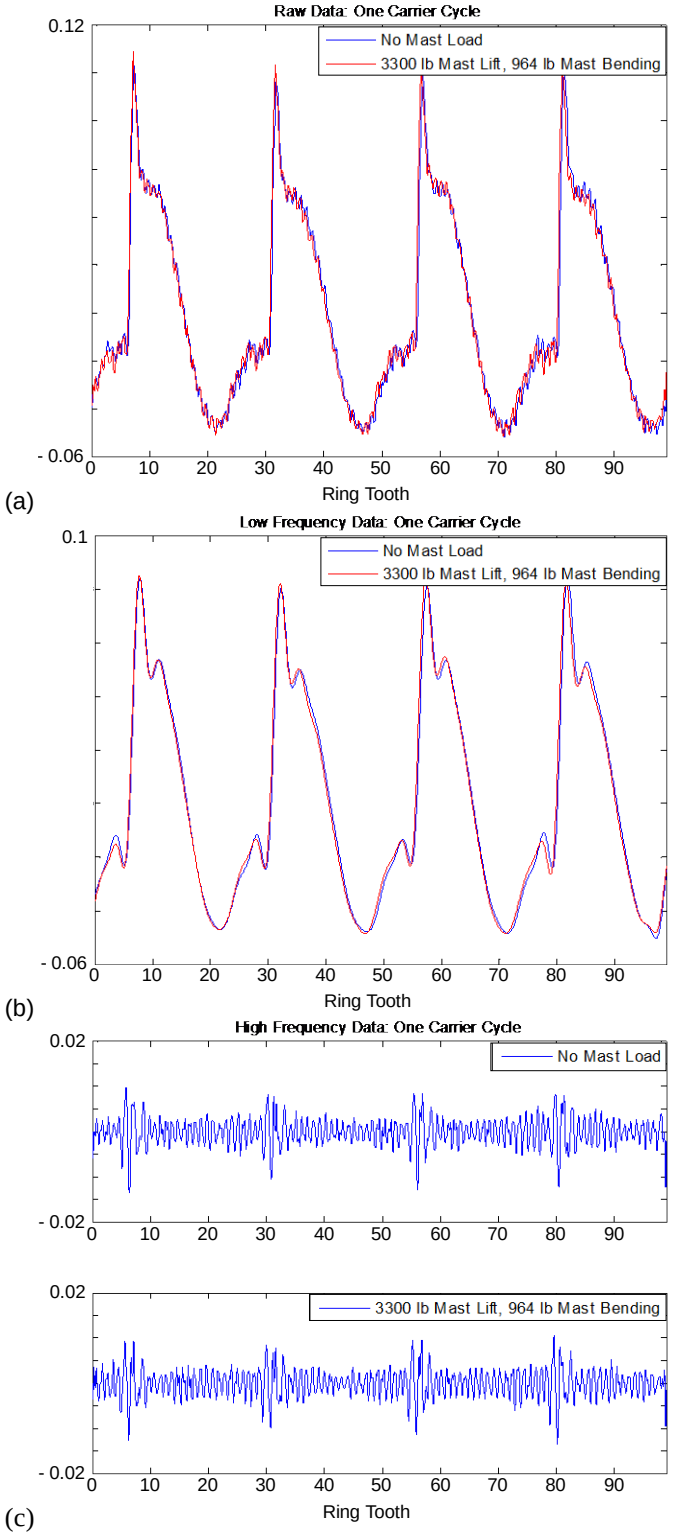

Figure 14.—Comparison of 1-carrier cycle raw vibration signal for mast load off and mast load on conditions. (a) Raw signal, (b) low frequency component, (c) high frequency component

Mast Loading Sensitivity

For each test case investigated in this project, data with the mast load both on and off were collected. The mast load in this project consisted of both a mast lift and mast bending load applied simultaneously. For the previous results, the case with no mast load was used.

Figure 14(a) shows unaveraged vibration signals for the mast load on and off cases for a single carrier cycle. Figure 14(b) shows the low frequency component of the signals, and Figure 14(c) shows the high frequency component of the signals. From these figures, it appears that the mast load has a negligible effect on the raw strain signal as well as both the high and low frequency components of the signal. Calculation of the condition indicators confirms that mast loading does not affect damage detection.

Summary and Conclusion

This paper is focused on the use of a Fiber Optic Strain Sensor Array for detecting damage in the planetary stage of a helicopter transmission. A removable band-type of sensor was developed for use with fiber Bragg grating sensors. With modifications to the ring gear and transmission housing, the sensor array was installed on a Bell OH-58C transmission at the NASA Glenn Helicopter Transmission Test Facility.

Testing of the fiber optic sensor array was performed throughout a series of tests that consisted of baseline and multiple damage cases including cracks and spalls of the planetary gears. Testing of each damage case was performed over a range of torque loads with and without mast loading. Analysis of the resulting strain signals shows extremely repeatable measurements with high signal-to-noise ratio as compared to conventional accelerometer measurements.

Damage detection was performed on the high frequency component of the strain signal using condition indicators previously developed for accelerometer-based measurements. Using these indicators, the fiber optic strain measurements are capable of detecting several types of damage including planet gear cracks and spalls. However the technique shows limitation in detecting other damage cases such as damaged sun gears and bearing race pitting.

The fiber optic strain measurements also show strong correlation with torque loading. Although this leads to a decreased damage sensitivity at low torque levels, it also provides a potential new type of torque measurement technique. No effect was detected with mast loading.

References

1. Giurgiutiu, V., Cuc, A., and Goodman, P., “Review of Vibration-Based Helicopters Health and Usage Monitoring Methods,” Proceeding of the 55th Meeting of the Society for Machinery Failure Prevention Technology, April 2–5, 2001, Virginia Beach, VA.

2. Zakrajsek, J., et al., “Rotorcraft Health Management Issues and Challenges,” prepared for the First International Forum on Integrated System Health Engineering and Management in Aerospace, cosponsored by NASA Ames Research Center and Marshall Space Flight Center, Napa, CA, Nov. 7–10, 2005, NASA/TM—2006-214022.
3. Samuel, P., and Pines, D., “A Review of Vibration Based Techniques for Helicopter Transmission Diagnostics,” Journal of Sound and Vibration, Vol. 282, 2005, pp. 475–508.
4. Othonos, A., and Kalli, K., “Fiber Bragg Gratings: Fundamentals and Applications in Telecommunications and Sensing,” Artech House, Inc., London, United Kingdom, ISBN 0-89006-344-3, 1999.
5. Baldwin, C., Kiddy, J., Samuel, P., Coker, J., and Pines, D., “Fiber Optic Sensors Monitoring Transmission Ring Gears,” Proceedings of the SPIE Optics East Conference, Boston, MA, 2007.
6. Coker, J., Pines, D., Samuel, P., Kiddy, J. and Baldwin, C., “Fiber Bragg Gratings for Detection of Planetary Gear Damage in Helicopter Transmissions,” Proceedings of the Fifth International Conference on Condition Monitoring and Machinery Failure Prevention Technology, Edinburgh, United Kingdom, 2008.
7. Coker, J., Pines, D., Samuel, P.D., and Kiddy, J., 2008, “Fiber Optic Strain Sensor Vibration Separation for Detection of Seeded Faults in Rotorcraft Transmissions,” Proceedings of the ASME SMASIS Conference, Ellicott City, MD.
8. Lewicki, D., and Woods, R., “Evaluation of Low-Noise, Improved-Bearing-Contact Spiral Bevel Gears,” Proceedings of the 59th American Helicopter Society Annual Forum, Phoenix, AZ, May 2003.
9. R. Kashyap: Fiber Bragg Gratings, Academic Press, San Diego, CA, 1999.
10. Samuel, P., “Helicopter Transmission Diagnostics using Constrained Adaptive Lifting,” Ph.D. Dissertation, University of Maryland, College Park, MD, Aug. 2003.
11. McFadden, P., “A Technique for Calculating the Time Domain Averages of the Vibration of the Individual Planet Gears and Sun Gear in an Epicyclic Gearbox,” Journal of Sound and Vibration, Vol. 144, (1), 1991, pp. 163–172.
12. Samuel, P. and Pines, D., “Vibration Separation and Diagnostics of Planetary Geartrains,” Proceedings of the AHS 56th Forum, Virginia Beach, VA, May 2–4, 2000.
13. Decker, H., and Zakrajsek, J., “Comparison of Interpolation Methods as Applied to Time Synchronous Averaging,” NASA/ARL Technical Report, NASA/TM—1999-209086, ARL–TR–1960, 1999.

REPORT DOCUMENTATION PAGE	Form Approved OMB No. 0704-0188

1. REPORT DATE *(DD-MM-YYYY)*	2. REPORT TYPE	3. DATES COVERED *(From - To)*
01-11-2011	Technical Memorandum	

4. TITLE AND SUBTITLE
Fiber Optic Strain Sensor for Planetary Gear Diagnostics

5a. CONTRACT NUMBER

5b. GRANT NUMBER

5c. PROGRAM ELEMENT NUMBER

6. AUTHOR(S)
Kiddy, Jason, S.; Samuel, Paul, D.; Lewicki, David, G.; LaBerge, Kelsen, E.; Ehinger, Ryan, T.; Fetty, Jason

5d. PROJECT NUMBER

5e. TASK NUMBER

5f. WORK UNIT NUMBER
WBS 877868.02.07.03.01.01.01

7. PERFORMING ORGANIZATION NAME(S) AND ADDRESS(ES)
National Aeronautics and Space Administration
John H. Glenn Research Center at Lewis Field
Cleveland, Ohio 44135-3191

8. PERFORMING ORGANIZATION REPORT NUMBER
E-17812

9. SPONSORING/MONITORING AGENCY NAME(S) AND ADDRESS(ES)
National Aeronautics and Space Administration
Washington, DC 20546-0001

10. SPONSORING/MONITOR'S ACRONYM(S)
NASA

11. SPONSORING/MONITORING REPORT NUMBER
NASA/TM-2011-217123

12. DISTRIBUTION/AVAILABILITY STATEMENT
Unclassified-Unlimited
Subject Category: 37
Available electronically at http://www.sti.nasa.gov
This publication is available from the NASA Center for AeroSpace Information, 443-757-5802

13. SUPPLEMENTARY NOTES

14. ABSTRACT
This paper presents a new sensing approach for helicopter damage detection in the planetary stage of a helicopter transmission based on a fiber optic strain sensor array. Complete helicopter transmission damage detection has proven itself a difficult task due to the complex geometry of the planetary reduction stage. The crowded and complex nature of the gearbox interior does not allow for attachment of sensors within the rotating frame. Hence, traditional vibration-based diagnostics are instead based on measurements from exter-nally mounted sensors, typically accelerometers, fixed to the gearbox exterior. However, this type of sensor is susceptible to a number of external disturbances that can corrupt the data, leading to false positives or missed detection of potentially catastrophic faults. Fiber optic strain sensors represent an appealing alternative to the accelerometer. Their small size and multiplexibility allows for potentially greater sensing resolution and accuracy, as well as redundancy, when employed as an array of sensors. The work presented in this paper is focused on the detection of gear damage in the planetary stage of a helicopter transmission using a fiber optic strain sensor band. The sensor band includes an array of 13 strain sensors, and is mounted on the ring gear of a Bell Helicopter OH-58C transmission. Data collected from the sensor array is compared to accelerometer data, and the damage detection results are presented.

15. SUBJECT TERMS
Transmissions (machine element); Fiber optics; Gears; Detection

16. SECURITY CLASSIFICATION OF:			17. LIMITATION OF ABSTRACT	18. NUMBER OF PAGES	19a. NAME OF RESPONSIBLE PERSON
a. REPORT	b. ABSTRACT	c. THIS PAGE			STI Help Desk (email:help@sti.nasa.gov)
U	U	U	UU	22	19b. TELEPHONE NUMBER *(include area code)* 443-757-5802